Supporting Information

Stretchable high response piezoelectric elastomers based on polable polynorbornene fillers in a polydimethylsiloxane matrix

Francis Owusu, Frank A. Nüesch, and Dorina M. Opris**

((Optional Dedication))

Francis Owusu, Frank A. Nüesch, and Dorina M. Opris
Laboratory for Functional Polymers, Swiss Federal Laboratories for Materials Science and Technology Empa, Überlandstrasse 129 CH-8600 Dübendorf, Switzerland.
E-mail:
francis.owusu@empa.ch
dorina.opris@empa.ch

Francis Owusu
Institute of Chemical Sciences and Engineering, Ecole Polytechnique Federale de Lausanne (EPFL), Station 6 CH-1015 Lausanne, Switzerland

Frank A. Nüesch
Institute of Materials Science and Engineering, Ecole Polytechnique Federale de Lausanne (EPFL), Station 6 CH-1015 Lausanne, Switzerland

Table of Contents

Synthesis Route

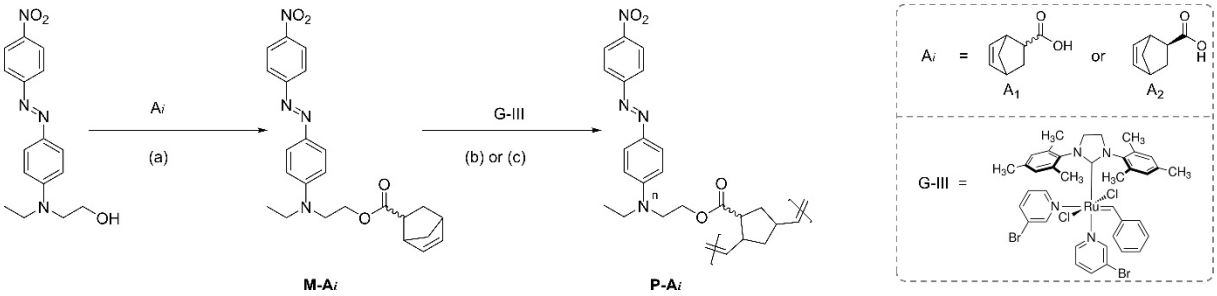

Scheme S1 Synthesis of **M-Ai** and respective **P-Ai**: (a) 4-dimethylaminopyridine (DMAP), N,N'-dicyclohexylcarbodiimide (DCC), dry dichloromethane (DCM), 24 h, 45 °C. Grubbs 3rd generation catalysts (G-III), dry DCM; (b) **M-A1**, 40 °C for 23 h (c) **M-A2**, 25°C for 2 h.

Synthesis of M-Ai: A dried 2-necked round bottom flask was charged with ether 5-norbornene-2-carboxylic acid, mixture of *endo* and *exo*, predominantly *endo* (**A1**) or *exo*-5-norbornene-2-carboxylic acid (**A2**) (5.00 g, 36.202 mmol), *N*-ethyl-*N*-(2-hydroxyethyl)-4-(4-nitrophenylazo) aniline (11.38 g, 36.20 mmol) and 4-dimethylaminopyridine (8.85 g, 72.40 mmol) dissolved in of anhydrous DCM (60 mL). N,N'-dicyclohexylcarbodiimide (14.94 g, 72.40 mmol) was added at 0 °C to the reaction mixture, stirred for 5 min at 0 °C, and refluxed for 24 h at 45 °C. The resulting crude mass was concentrated in vacuum and purified using column chromatography with heptane and ethyl acetate (3:2) mixture as eluent.

M-A1 was obtained as a reddish powder (95 % yield): ^{1}H NMR (400 MHz, $CDCl_3$) δ 8.43 – 8.24 (m, 2H), 8.04 – 7.82 (m, 4H), 6.90 – 6.74 (m, 2H), 6.24 – 6.13 (m, 1H), 6.01 (ddd, J = 77.5, 5.7, 3.0 Hz, 1H), 4.30 (dt, J = 26.8, 6.3 Hz, 2H), 3.70 (dt, J = 15.8, 6.3 Hz, 2H), 3.56 (q, J = 7.2 Hz, 2H), 3.24 – 3.10 (m, 1H), 3.05 – 2.87 (m, 2H), 2.02 – 1.89 (m, 2H), 1.44 (ddd, J = 11.1, 7.6, 4.1 Hz, 2H), 1.28 (t, J = 7.1 Hz, 3H). ^{13}C NMR (101 MHz, $CDCl_3$) δ 175.69 (d, J = 106.1 Hz), 174.71, 156.76, 151.32, 147.36, 143.82, 138.14, 138.02, 136.86, 135.63, 132.53, 132.19, 126.27, 124.66, 122.64, 111.47, 61.32, 61.18, 55.94, 55.74, 49.81, 49.76, 49.70, 48.85, 48.79, 46.81, 46.57, 46.39, 45.71, 45.65, 45.61, 44.36, 43.31, 43.08, 42.75, 42.54, 41.63, 34.94, 33.97, 32.87, 32.80, 31.27, 31.14, 30.85, 30.44, 29.29, 26.48, 26.41, 25.53, 25.47, 25.40, 24.99, 24.86, 24.70, 12.30.

M-A2 was obtained as a reddish powder (91 % yield): ^{1}H NMR (400 MHz, $CDCl_3$) δ 8.39 – 8.30 (m, 2H), 8.00 – 7.88 (m, 4H), 6.89 – 6.79 (m, 2H), 6.18 – 6.09 (m, 2H), 4.34 (t, *J* = 6.3 Hz, 2H), 3.72 (t, *J* = 6.3 Hz, 2H), 3.57 (q, *J* = 7.1 Hz, 2H), 3.07 – 2.99 (m, 1H), 2.97 – 2.90 (m, 1H), 2.29 – 2.19 (m, 1H), 1.91 (dt, *J* = 11.8, 4.0 Hz, 1H),1.52 (dt, *J* = 8.3, 1.6 Hz, 1H), 1.39 (dddd, *J* = 9.7, 8.4, 5.7, 2.6 Hz, 3H), 1.29 (t, *J* = 7.1 Hz, 3H). ^{13}C NMR (101 MHz, $CDCl_3$) δ

176.23, 156.62, 151.40, 147.44, 143.80, 138.52, 138.16, 136.07, 135.63, 126.41, 124.70, 122.62, 111.59, 61.30, 49.68, 48.91, 46.96, 46.84, 46.57, 46.40, 45.70, 43.79, 43.09, 41.72, 41.63, 32.88, 32.82, 32.08, 30.99, 30.86, 30.45, 26.53, 25.54, 25.37, 24.79, 12.31.

Polymerization Kinetics

Synthesis of P-Ai: Homopolymers of M-A*i* (M-A_1 and M-A_2) were prepared via ROMP with the same monomer-to-catalyst feed ratio ([M]:[C] = 400:1) and their rate of polymerization was studied. In an argon-filled Schlenk setup, a solution of M-A*i* (2.00 g, 4.603 mmol) in 30 mL of DCM, which was degassed in three freeze-vacuum-thaw cycles, was added to a degassed solution of G-III (10.18 mg, 0.012 mmol) in 16 mL of DCM to give a monomer concentration of 0.1 M. The reaction was allowed to proceed per conditions described in Scheme S1. The progress of polymerization was monitored at regular time intervals using ^{1}H NMR, done by taking aliquots and quenching with ethyl vinyl ether in $CDCl_3$. After confirming optimal monomer conversion by ^{1}H NMR, ethyl vinyl ether was added, and the resulting mixture was stirred for a further 1 h. The product mixture was concentrated under vacuum and then precipitated into excess methanol. The polymer was further purified by five consecutive dissolution (DCM) and re-precipitation cycles (MeOH). The obtained polymers were dried to constant weight under vacuum at 40 °C.

P-A_1 was obtained as a dark red solid: ^{1}H NMR(400 MHz, $CDCl_3$) δ: 8.26 (br d, J = 9.0 Hz, 2H), 7.87 (br s, 4H), 6.78 (br d, J = 12.2 Hz, 2H), 5.28 (br dd, J = 44.0, 21.3 Hz, 2H), 4.45–3.87 (br m, 2H), 3.56 (br d, J = 55.7 Hz, 4H), 3.26–2.61 (br m, 3H), 1.85 (br d, J = 86.3 Hz, 4H), 1.46–1.10 (br m, 3H). ^{13}C NMR (101 MHz, $CDCl_3$) δ: 174.28, 156.47, 154.00, 151.31, 147.31, 143.67, 134.52, 133.31, 132.48, 130.71, 129.80, 126.40, 124.64, 122.57, 111.50, 60.93, 50.12, 48.71, 45.61, 42.71, 40.51, 37.70, 36.10, 32.77, 31.11, 26.18, 25.45, 24.83, 12.36.

P-A_2 was obtained as a dark red solid: ^{1}H NMR (400 MHz, $CDCl_3$) δ 8.26 (br s, 2H), 7.86 (br s, 4H), 6.76 (br s, 2H), 5.25 (br d, J = 53.2 Hz, 2H), 4.25 (br s, 2H), 3.56 (br d, J = 60.4 Hz, 4H), 3.19 – 2.37 (br m, 3H), 2.17 – 1.47 (br m, 4H), 1.16 (br d, J = 40.5 Hz, 3H). ^{13}C NMR (101 MHz, $CDCl_3$) δ 175.36, 156.55, 151.27, 147.35, 143.73, 134.65, 133.55, 132.77, 131.99, 130.99, 126.40 126.33, 124.65, 122.62, 122.57, 111.48, 61.28, 50.40, 50.06, 49.63, 48.78, 45.67, 43.16, 41.94, 37.09, 32.81, 26.18, 25.43, 24.79, 12.33.

Theoretical consideration for calculating piezoelectric constants

The magnitude of charges, *Q*, per unit area, *A*, induced by the poled composite material on electrodes on the film surfaces is equal to the total macroscopic dipole moment, *M*, per unit volume, V, of polymer between the electrodes, which is the polarization, *P*. Thus;

$$\frac{Q}{A} = \frac{M}{V} = P$$

Eq. (1)

And

$$P = P_r + \Delta P$$

Eq. (2)

Where $P_r = \varepsilon_0 \Delta\varepsilon(T) E_p$, is the remnant polarization induced by poling and ΔP is the stress-induced polarization.

Piezoelectric charge coefficient, d_{31}, is the change in Q per unit area of the electrode on the poled sample with stress, S, applied perpendicularly in the cross-sectional direction; thus,

$$S = \frac{F}{A_c}$$

Eq. (3)

Where *F* is the applied force and A_c is the cross-sectional area where the force was applied.

$$d_{31} = \frac{\Delta Q}{S \cdot A_e} = \frac{\Delta Q \cdot A_c}{F \cdot A_e} = \frac{\Delta P \cdot A_c}{F}$$

Eq. (4)

Where A_e is area of the electrode on the poled sample.

Piezoelectric voltage coefficient, *g*, also called voltage output constant, is defined as the electric field, *E*, generated per unit of mechanical stress, *S*, applied and is expressed as

$$g = \frac{E}{S}$$

Eq. (5)

g_{31} and d_{31} are related to the relative permittivity from the equation:

$$g_{31} = \frac{d_{31}}{\varepsilon_r \varepsilon_0}$$

Eq. (6)

Where ε_r is the dielectric constant of the dielectric material and ε_0 is the permittivity of vacuum (8.85×10^{-12} F·m^{-1}).

The electromechanical coupling coefficient, k_{31}, represents the conversion efficiency between electrical and mechanical energy and is a measure of the combination of piezoelectric and mechanical properties of a material, expressed as:

$$k_{31} = d_{31}\sqrt{\frac{Y_{11}}{\varepsilon_r \varepsilon_0}}$$

Eq. (7)

Supplementary Figure

Kinetics Data on Polymerization

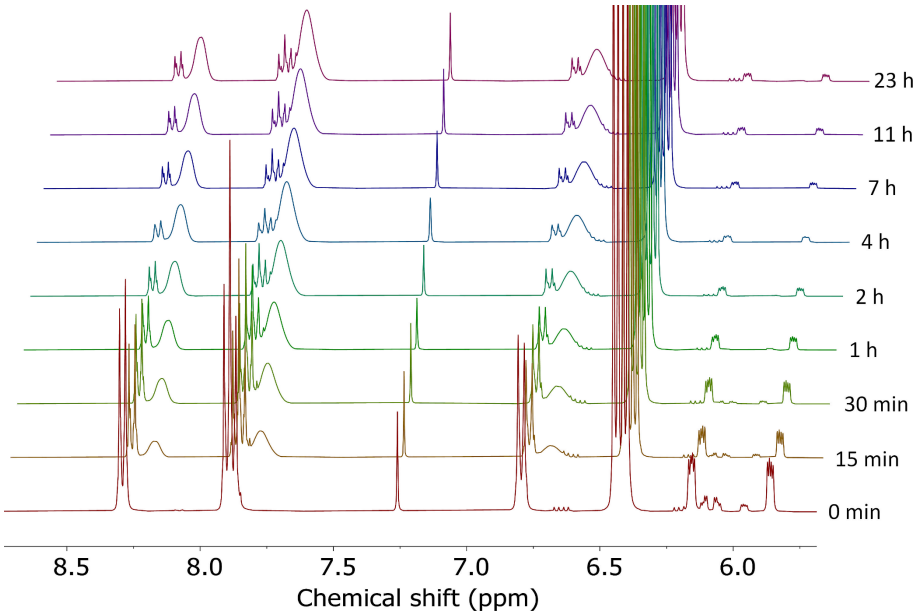

Figure S1 Stacked plot of ^{1}H NMR spectra for the kinetic progress of ROMP with [**M-A$_1$**]:[G-III] = 400:1

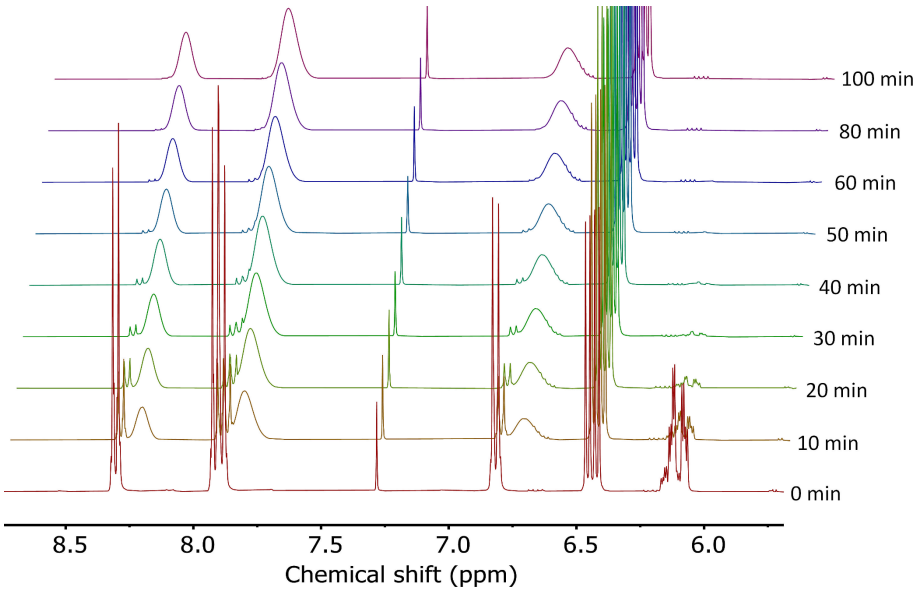

Figure S2 Stacked plot of ^{1}H NMR spectra for the kinetic progress of ROMP with [**M-A$_2$**]:[G-III] = 400:1

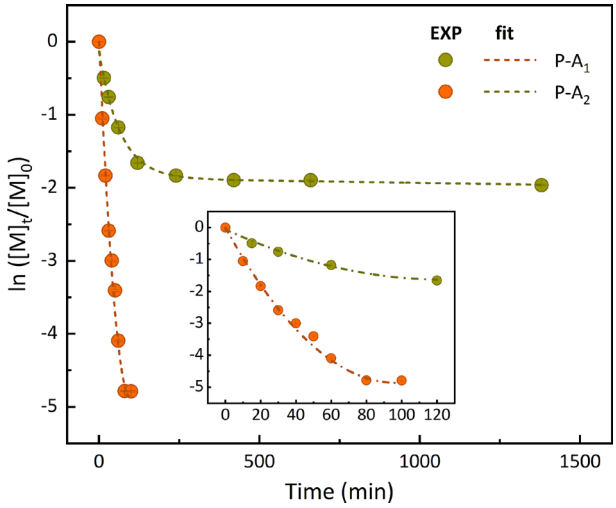

Figure S3 Plot of ln ([M]$_t$/[M]o) against time obtained from ^{1}H NMR spectra for **P-A$_1$** and **P-A$_2$**

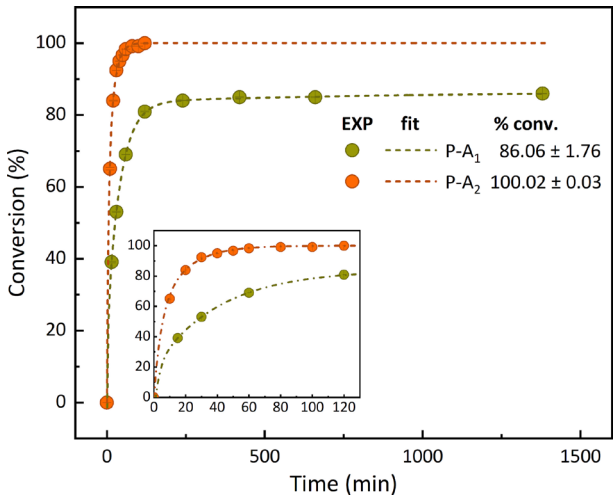

Figure S4 Percent conversion of **P-A$_1$** and **P-A$_2$** as a function of time as determined by ^{1}H NMR

Structure, Molecular Weight, and Thermal data

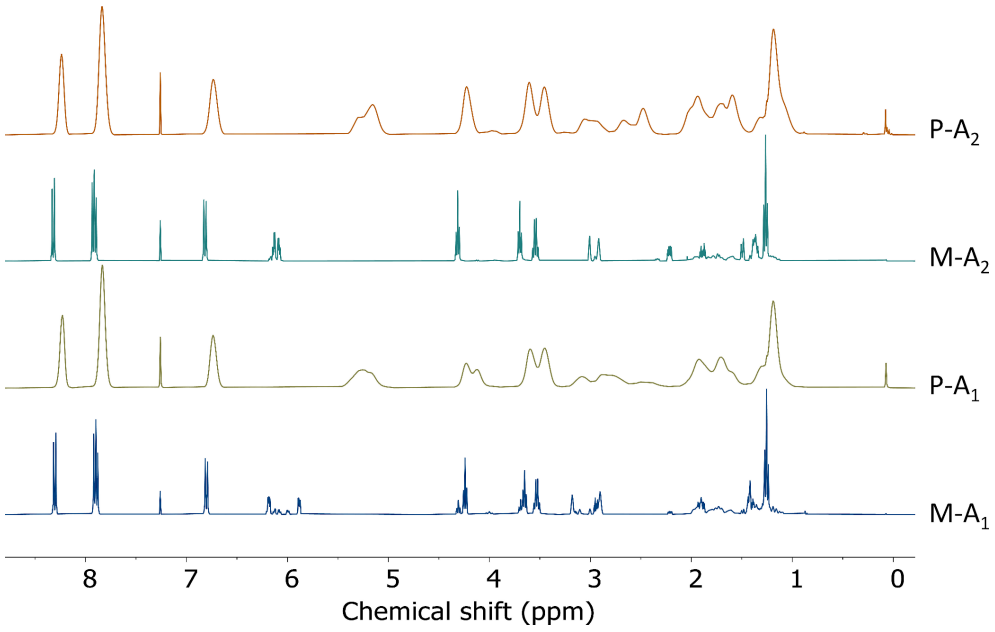

Figure S5 ^{1}H NMR spectra in $CDCl_3$ of monomers **M-A*i*** and their corresponding polymers **P-A*i***

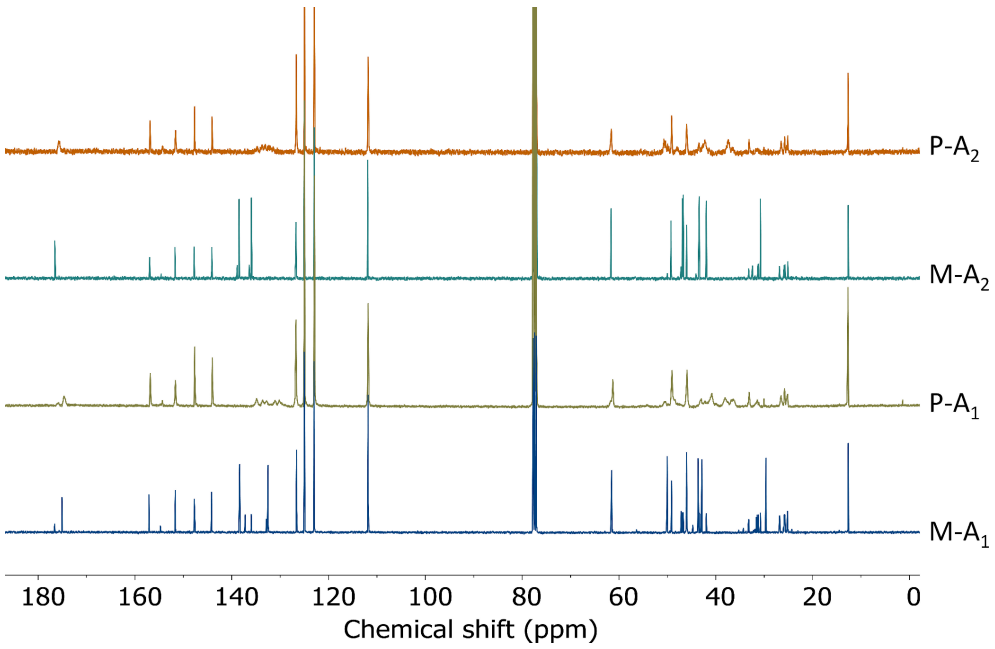

Figure S6 ^{13}C NMR spectra in $CDCl_3$ of monomers **M-A*i*** and their corresponding polymers **P-A*i***

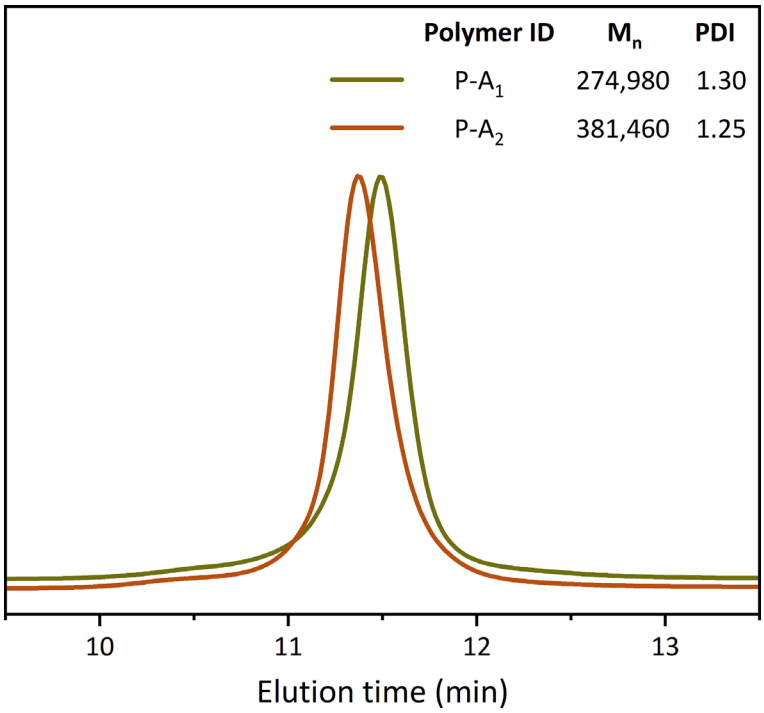

Figure S7 Normalized refractive index GPC traces of **P-A$_1$** and **P-A$_2$** in THF

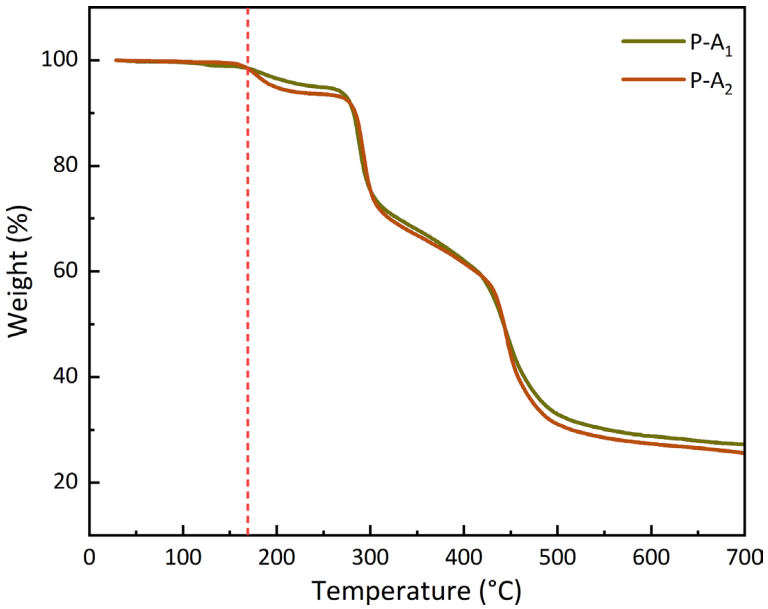

Figure S8 TGA thermograms of **P-A1** and **P-A2**. Both polymers showed stability up to 168 °C before yielding to thermal decomposition.

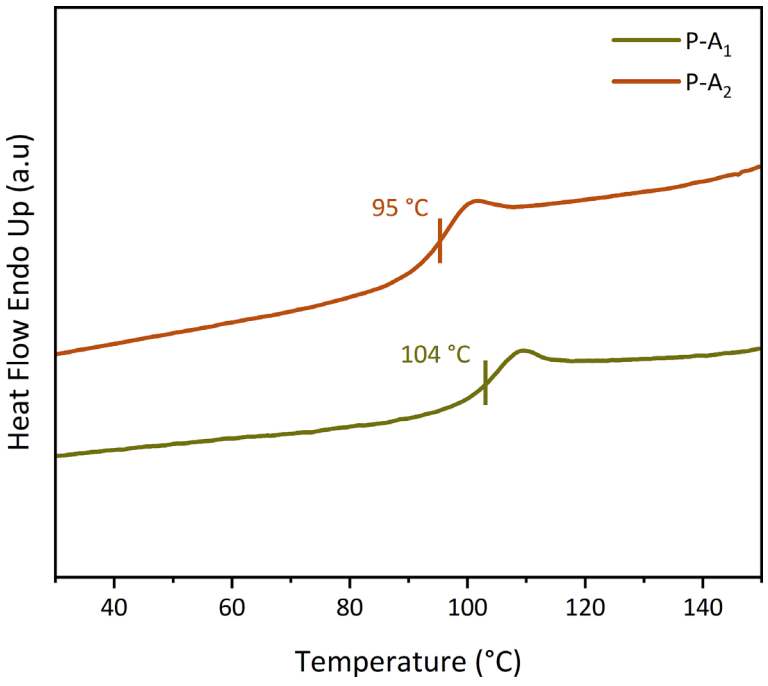

Figure S9 DSC curves of **P-A1** and **P-A2**

Composite Morphology evaluation

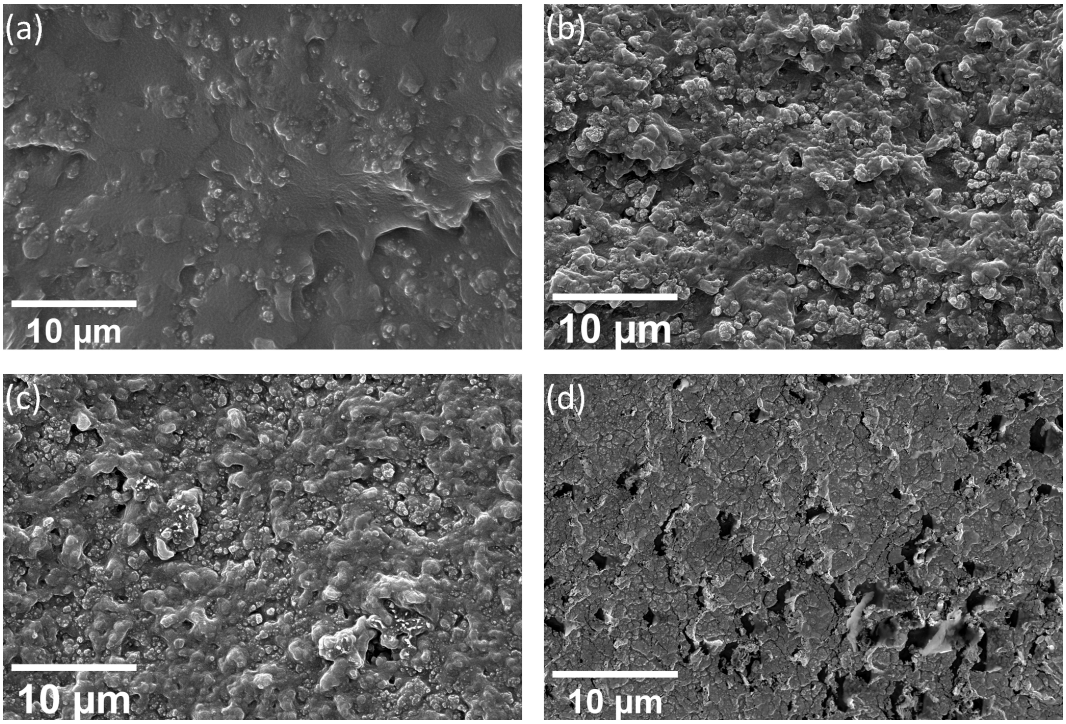

Figure S10 SEM image of the microstructure of composites prepared with P-$A_{1\text{-}s}$ filler in PDMS matrix with increasing filler content: (a) **P-$A_{1\text{-}s}$-10**; (b) **P-$A_{1\text{-}s}$-20**; (c) **P-$A_{1\text{-}s}$-30** and (d) **P-$A_{1\text{-}s}$-40**

Dielectric Spectra and TSDC Thermograms

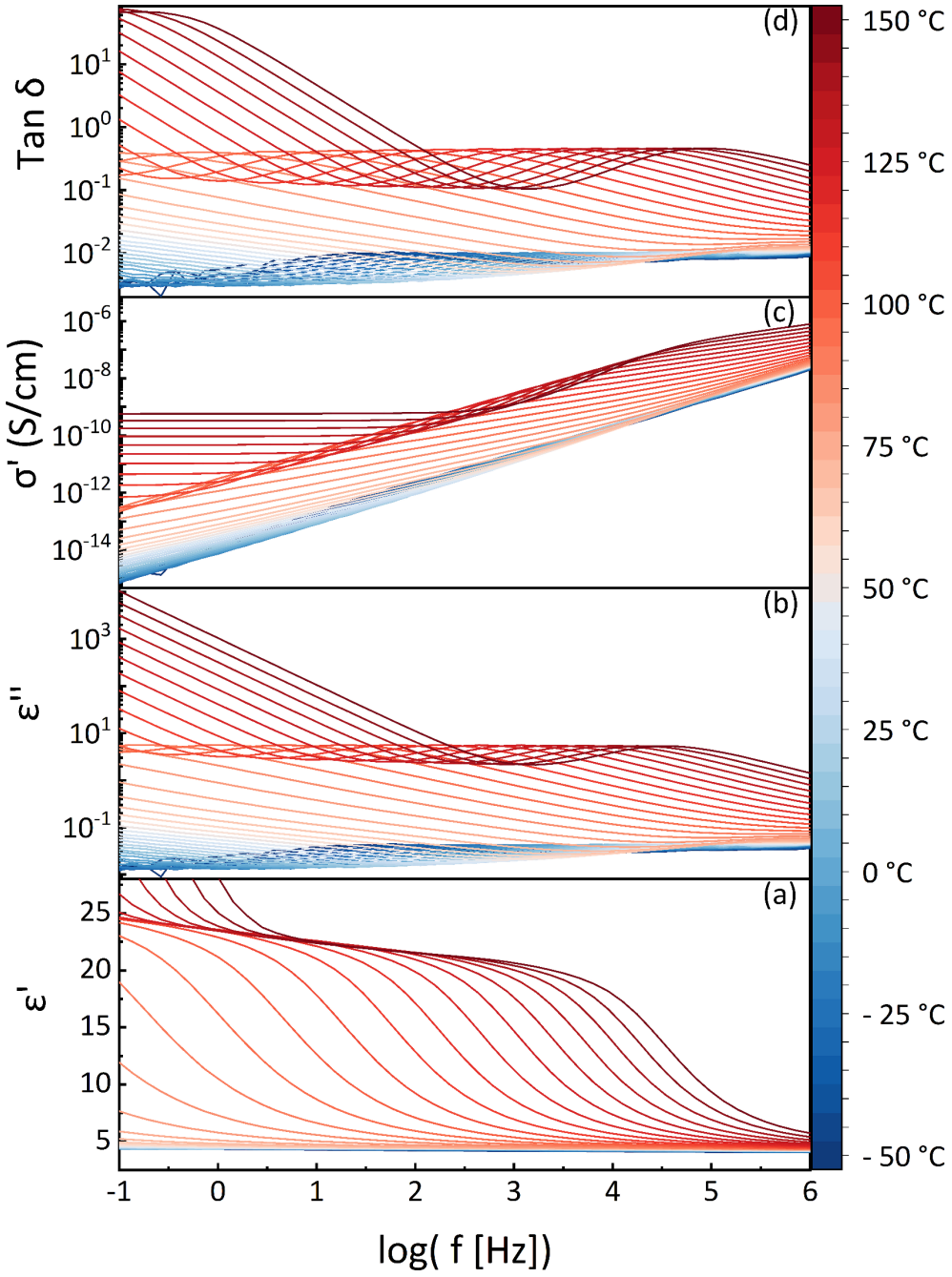

Figure S11 Isothermal dielectric response of **P-A$_1$** as a function of frequency: (a) real permittivity ε′; (b) dielectric loss ε″; (c) real conductivity σ′ and (d) loss tan δ.

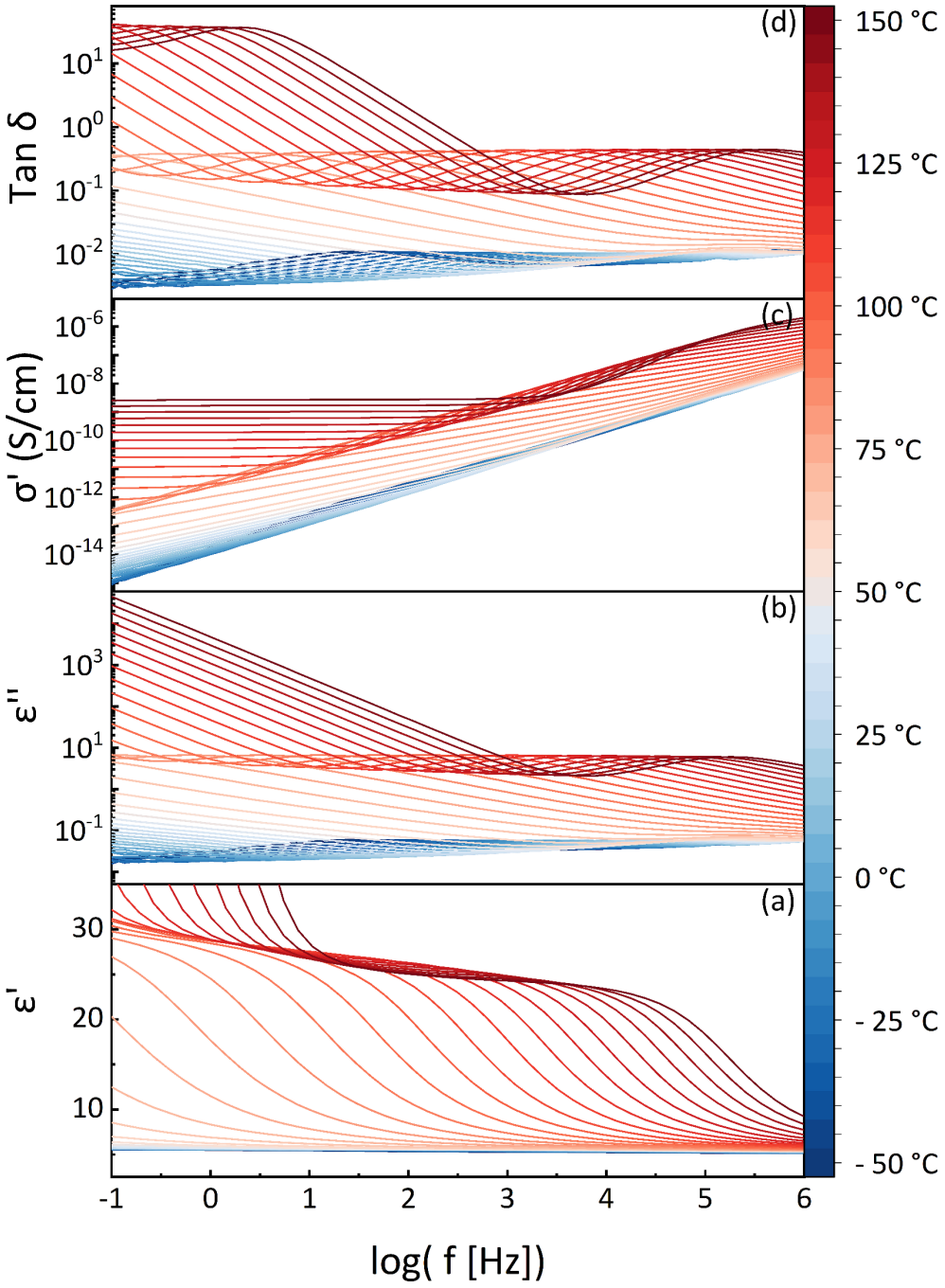

Figure S12 Isothermal dielectric response of **P-A$_2$** as a function of frequency: (a) real permittivity ε′; (b) dielectric loss ε′″; (c) real conductivity σ′ and (d) loss tan δ.

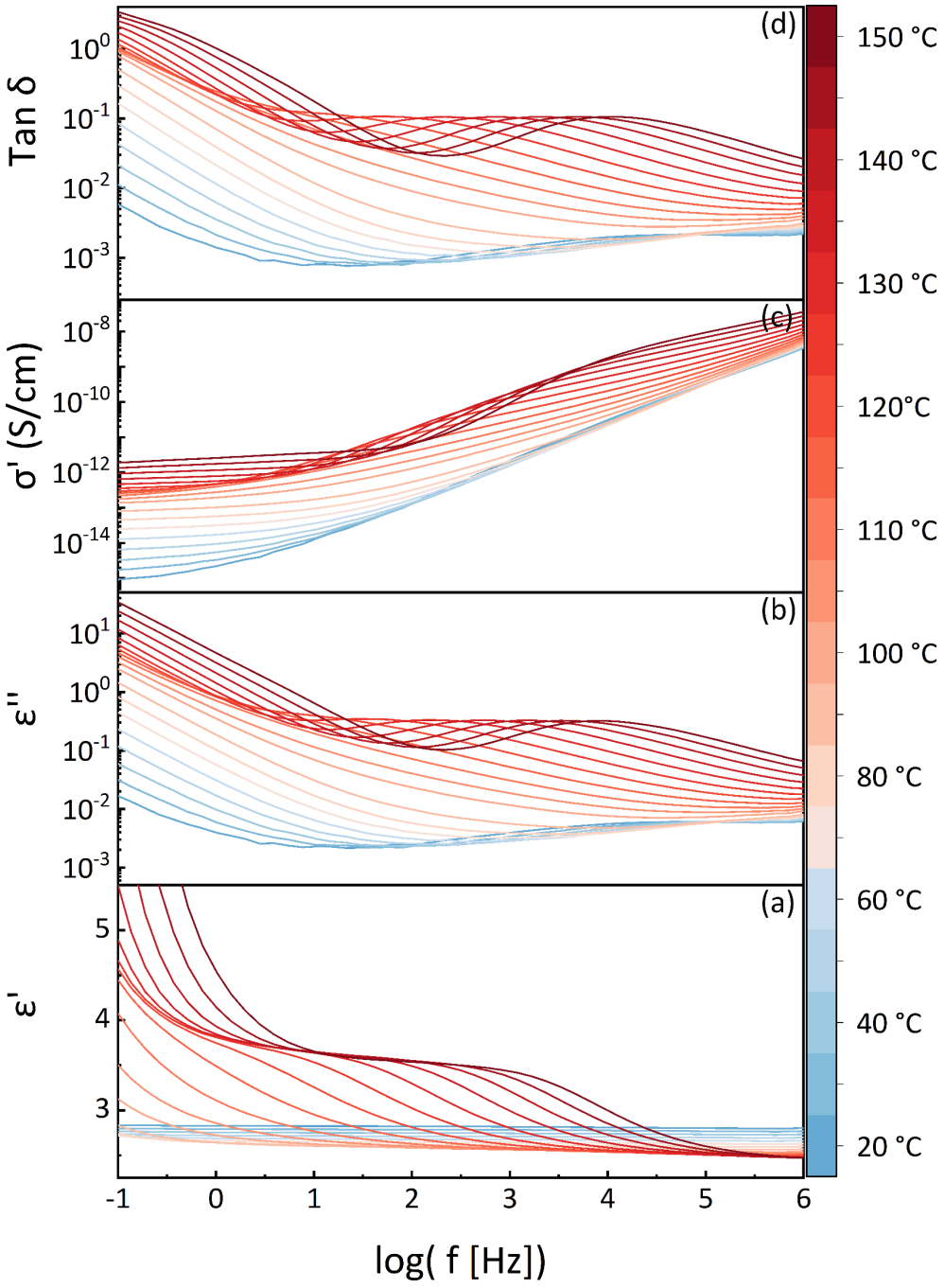

Figure S13 Isothermal dielectric response of **P-A$_{1\text{-}S}$ -30** as a function of frequency: (a) real permittivity ε; (b) dielectric loss ε″; (c) real conductivity σ′ and (d) loss tan δ.

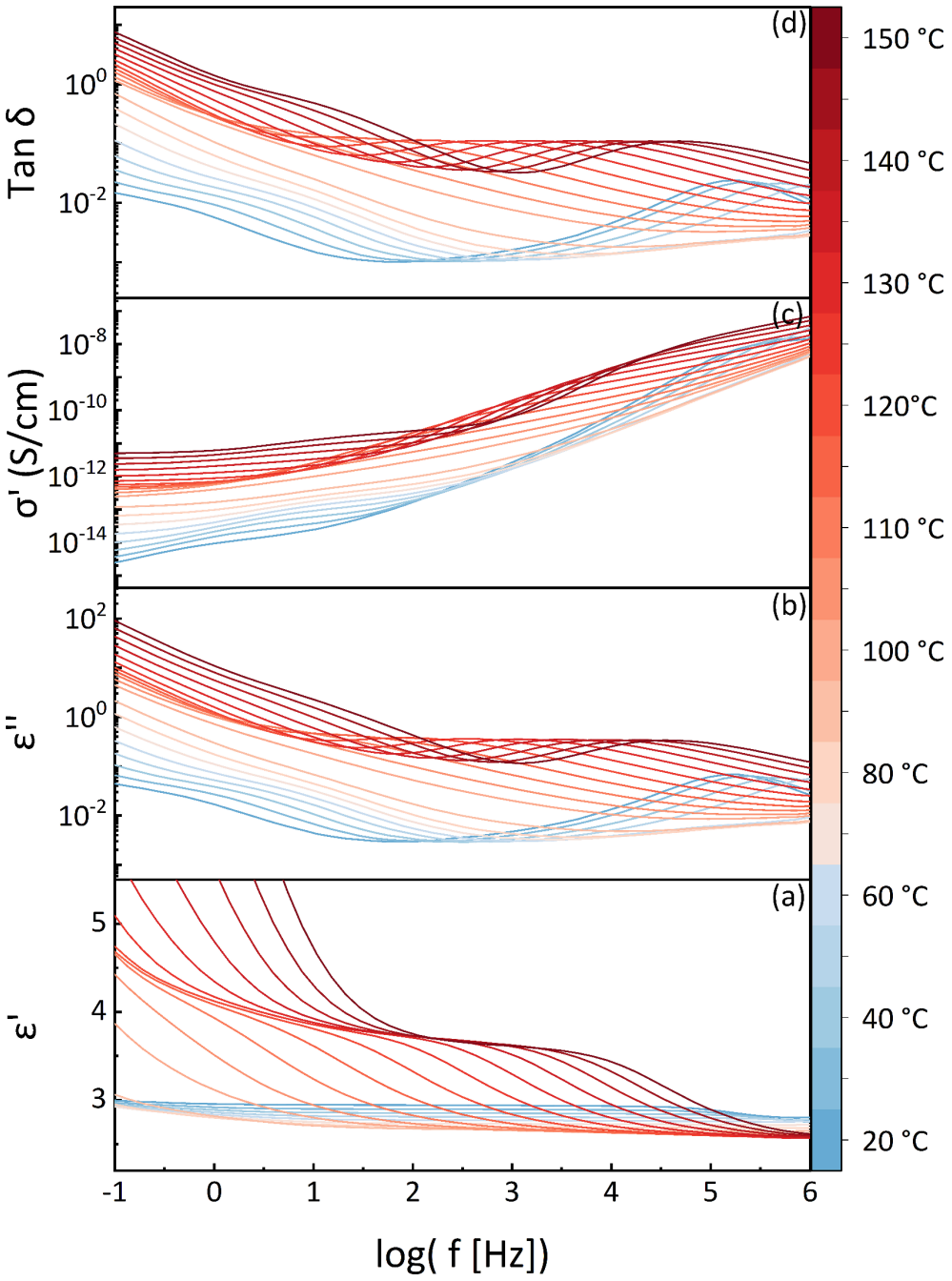

Figure S14 Isothermal dielectric response of **P-A$_{2\text{-}S}$ -30** as a function of frequency: (a) real permittivity ε′; (b) dielectric loss ε″; (c) real conductivity σ′ and (d) loss tan δ.

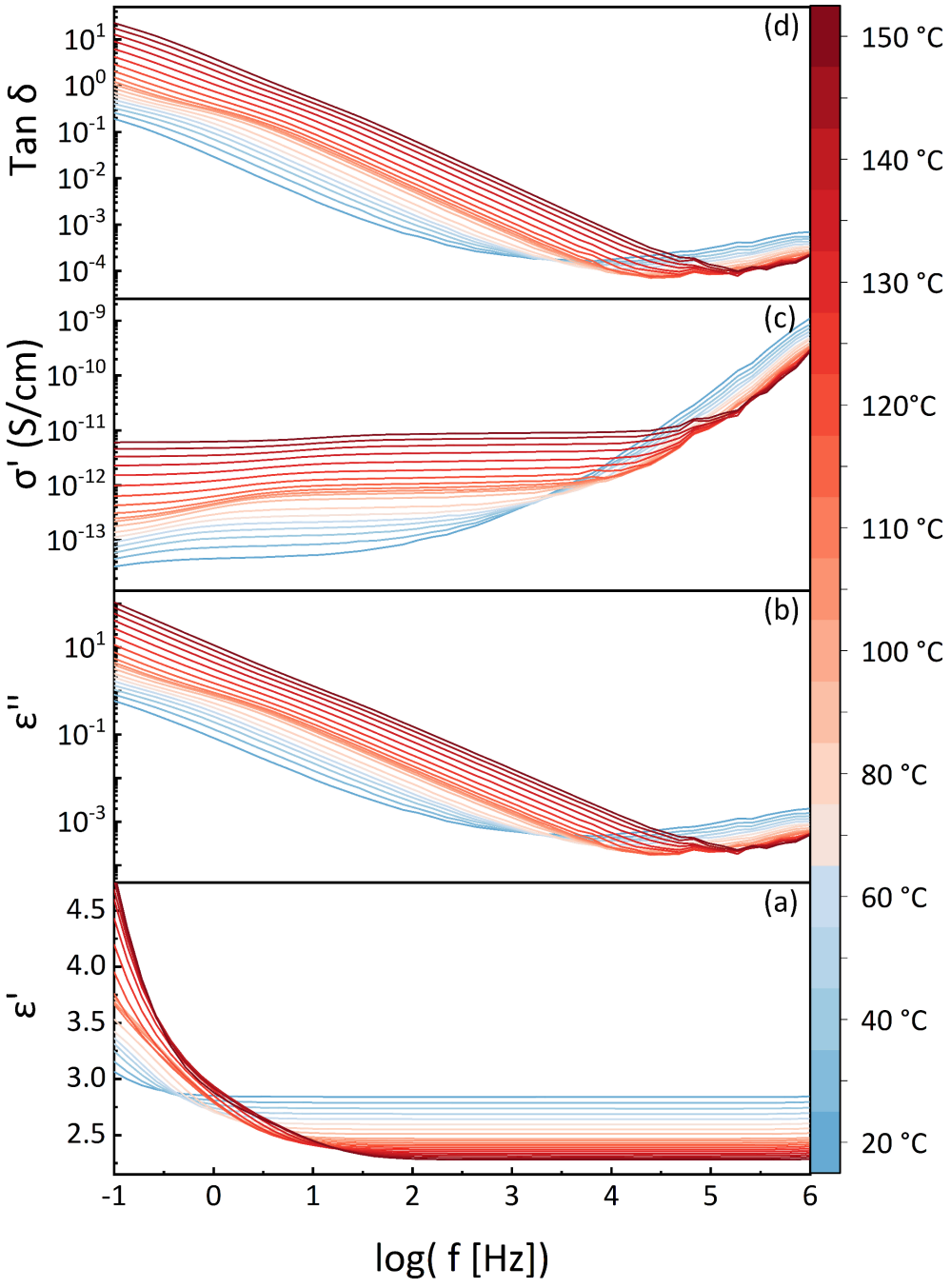

Figure S15 Isothermal dielectric response of PDMS matrix as a function of frequency: (a) real permittivity ε′; (b) dielectric loss ε″; (c) real conductivity σ′ and (d) loss tan δ.

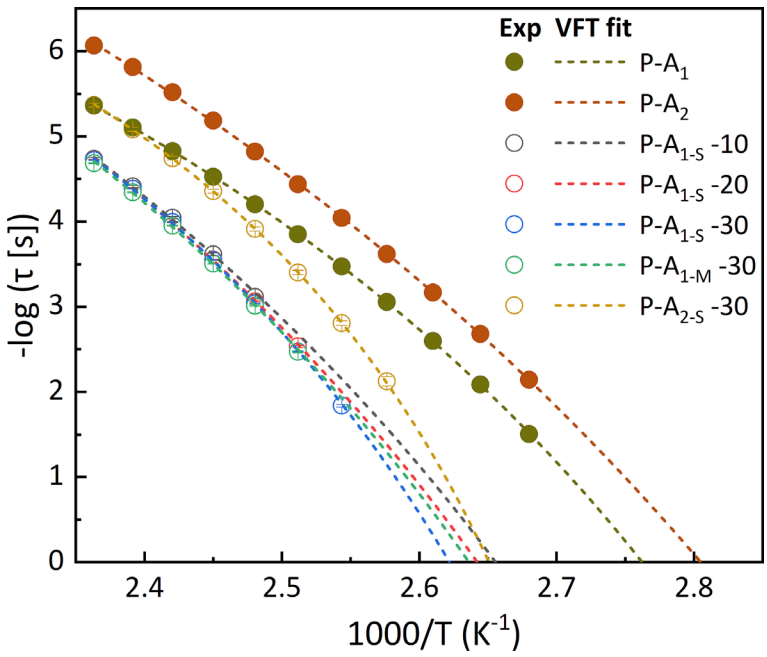

Figure S16 Effect of matrix on the dynamics of α-relaxation processes for polymers **P-A$_1$** and **P-A$_2$** with varying content in composites with PDMS. Vogel-Fulcher-Tammann (VFT) plot of corresponding relaxation times obtained from Havriliak-Negami (HN)-fit versus the inverse of temperature. Scattered dots represent the experimental data and the fit functions are represented by short-dashed lines

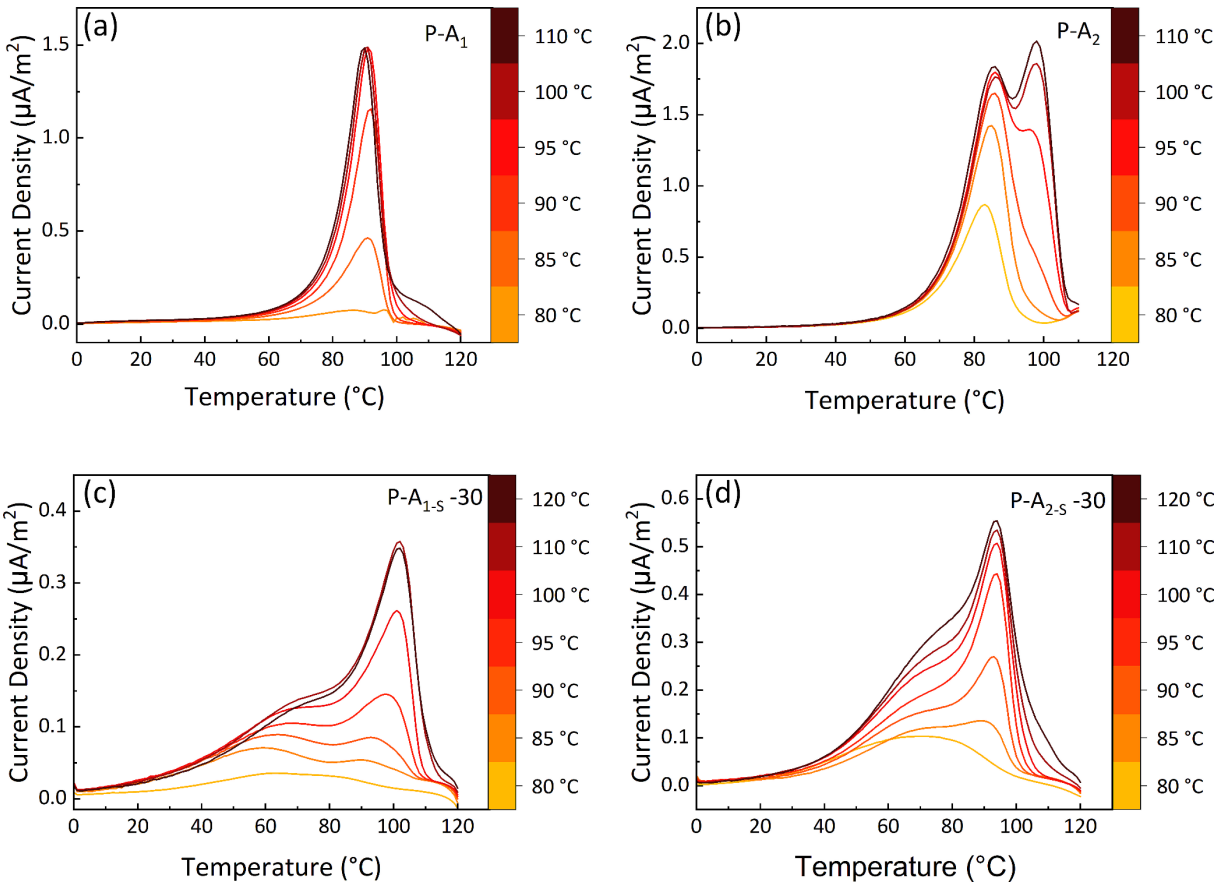

Figure S17 TSDC thermograms of (a) **P-A$_1$**; (b) **P-A$_2$**; (c) **P-A$_{1\text{-}S}$-30** and (d) **P-A$_{2\text{-}S}$-30**

Mechanical Property Data

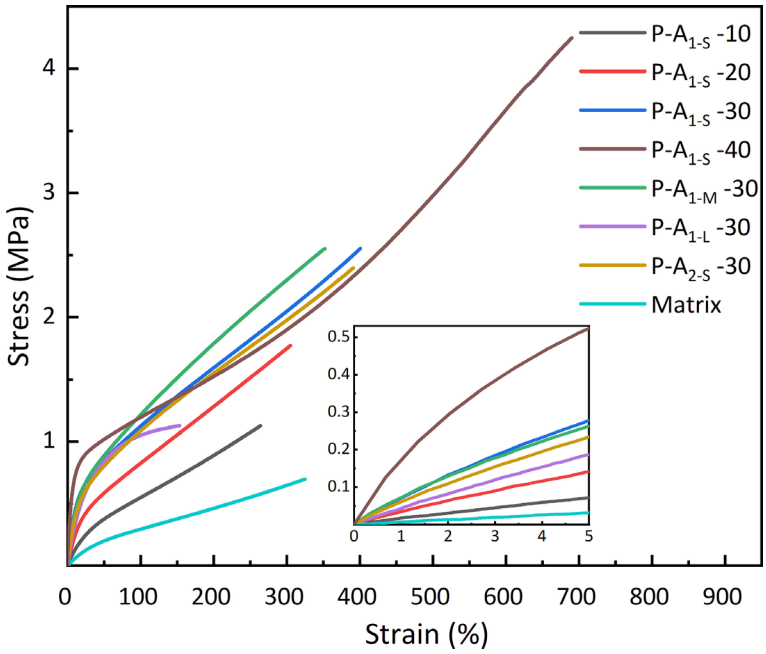

Figure S18 Uniaxial tensile curves of all the prepared composites and PDMS matrix. The average results of three independent measurements are as displayed.

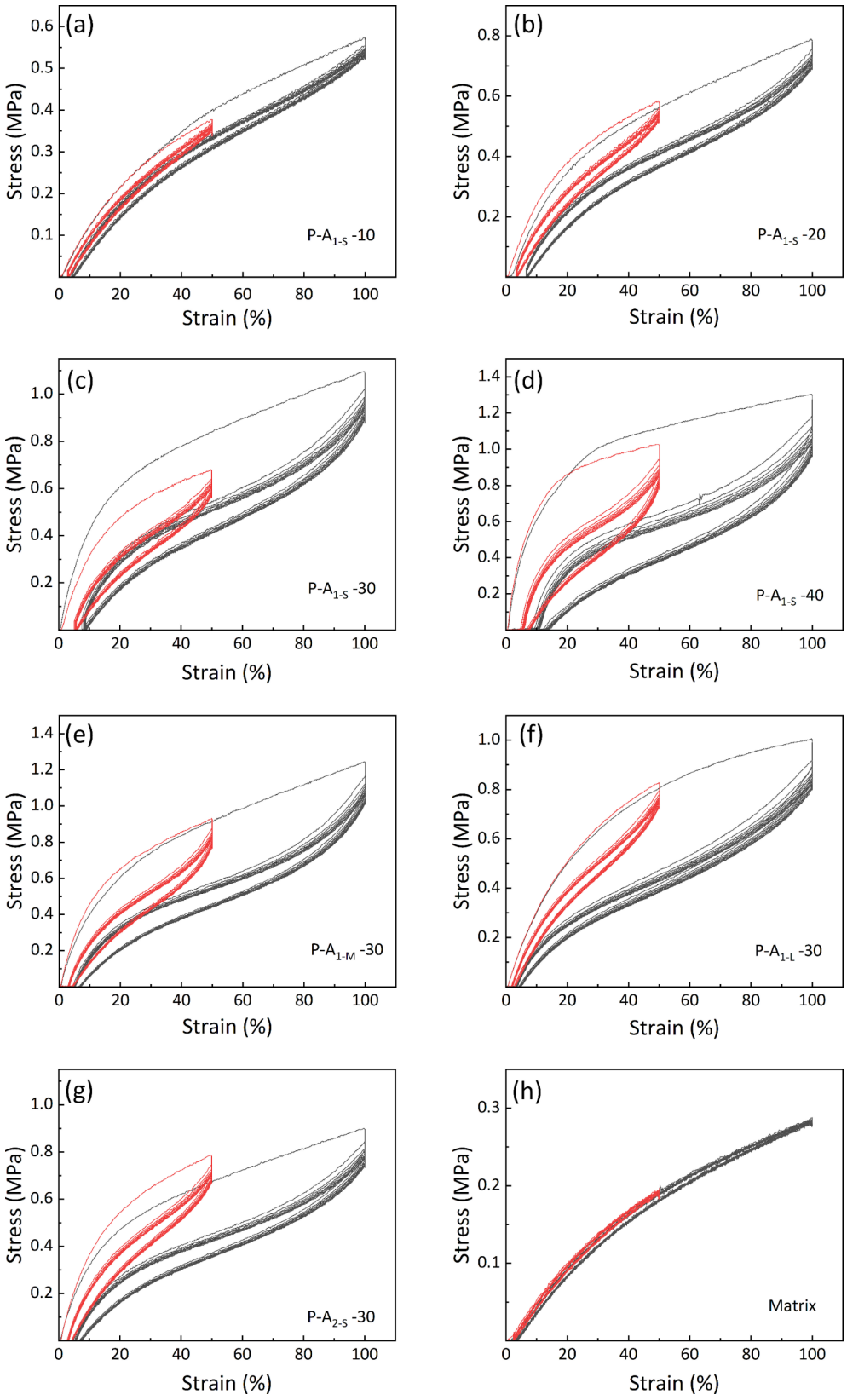

Figure S19 Representative uniaxial cyclic mechanical deformation of: (a) **P-A1-S -10**; (b) **P-A1-S -20**; (c) **P-A1-S -30**; (d) **P-A1-S -40**; (e) **P-A1-M -30**; (f) **P-A1-L -30**; (g) **P-A2-S -30**; (h) PDMS matrix

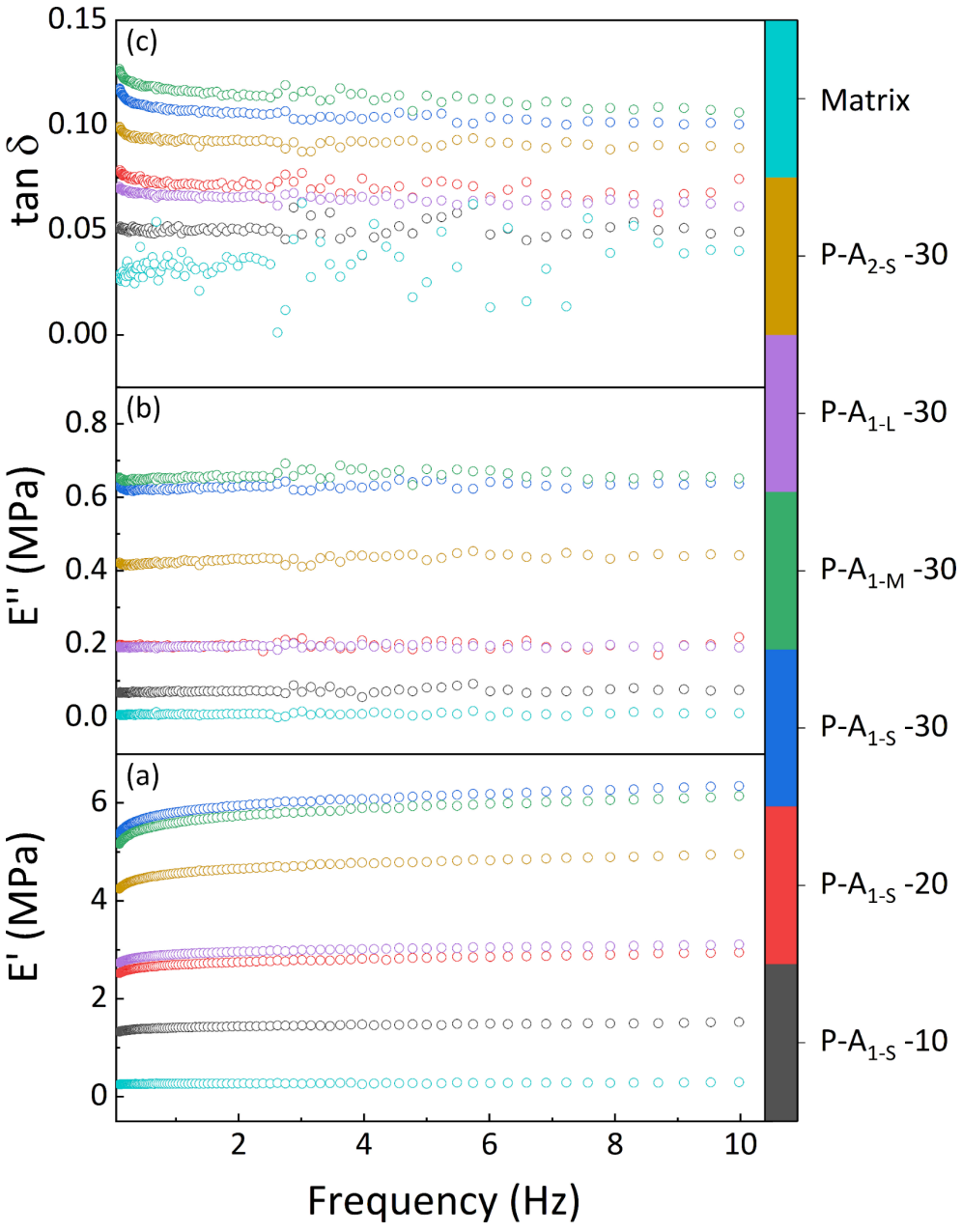

Figure S20 Frequency dependent DMA results obtained for composite materials and PDMS matrix: (a) storage modulus, *E′*; (b) loss modulus, *E″*; and (c) damping factor, *tan δ*.

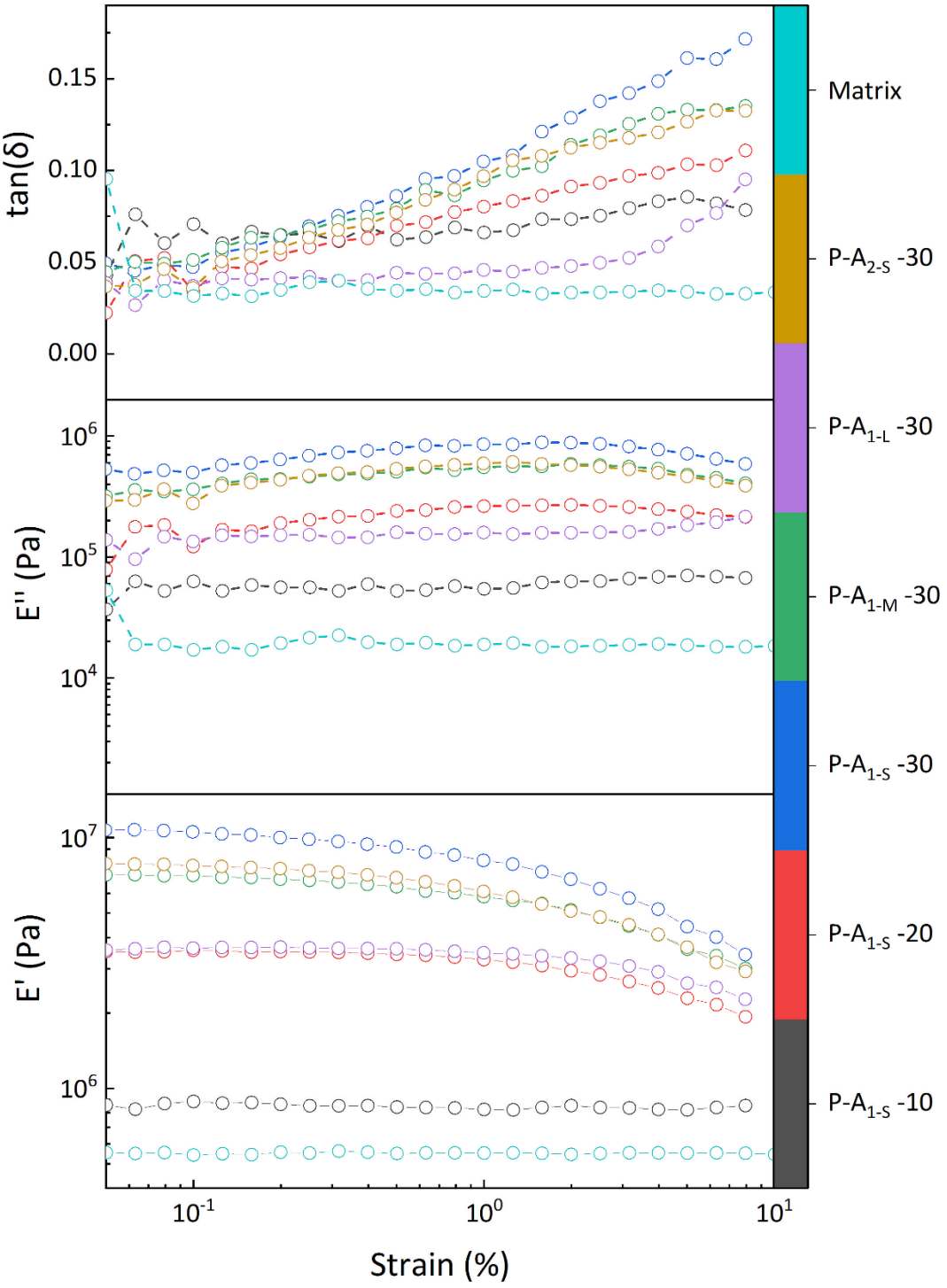

Figure S21 Strain dependent DMA results obtained for composite materials and PDMS matrix: (a) storage modulus, *E′*; (b) loss modulus, *E″*; and (c) damping factor, *tan δ*.

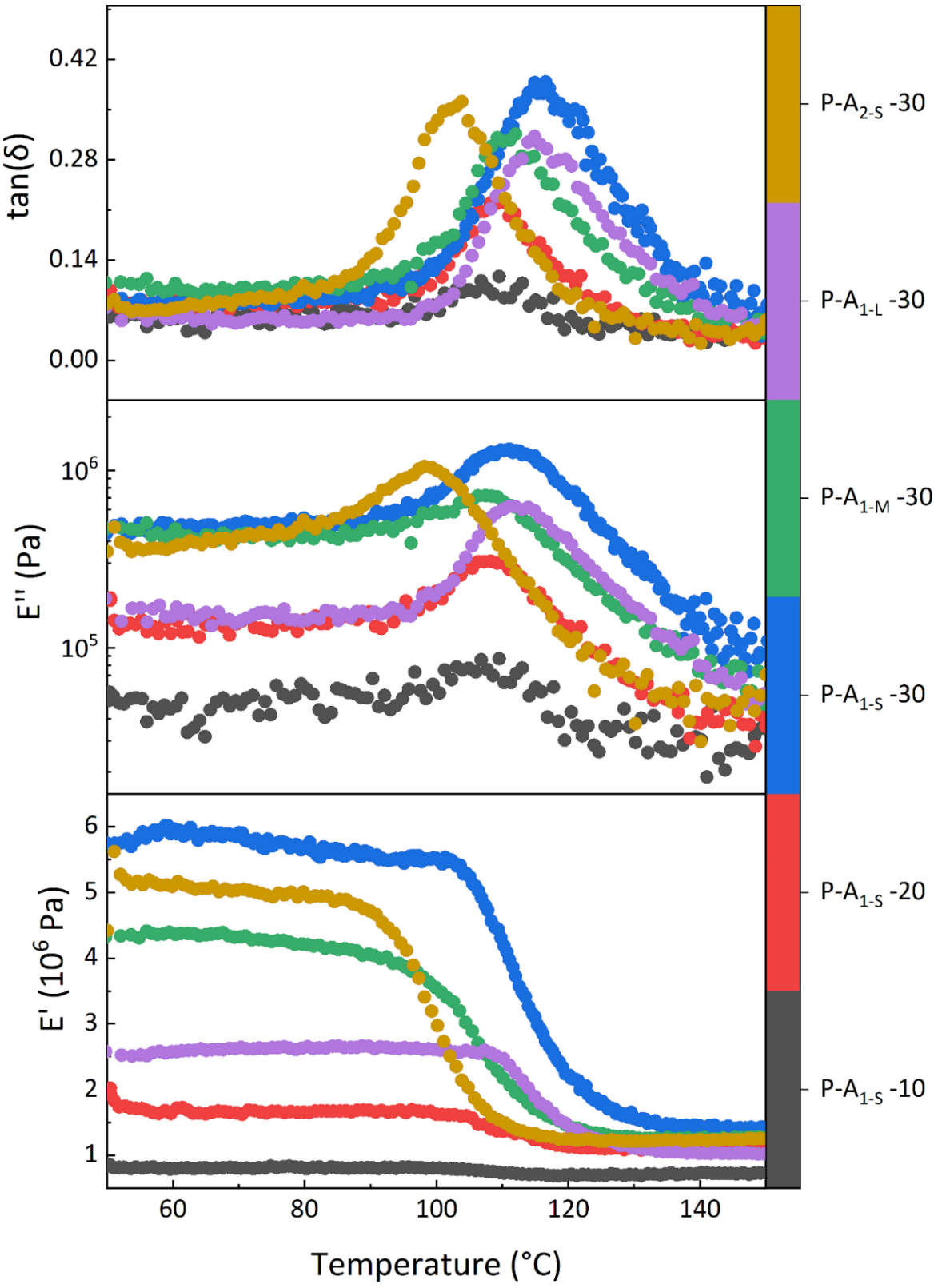

Figure S 22 Temperature dependent DMA for different materials were conducted by applying 0.5% strain at a frequency of 0.1 Hz: (a) storage modulus, E′; (b) loss modulus, E″; and (c) damping factor, tan δ.

Piezoelectric Coefficient (d_{31}) Data

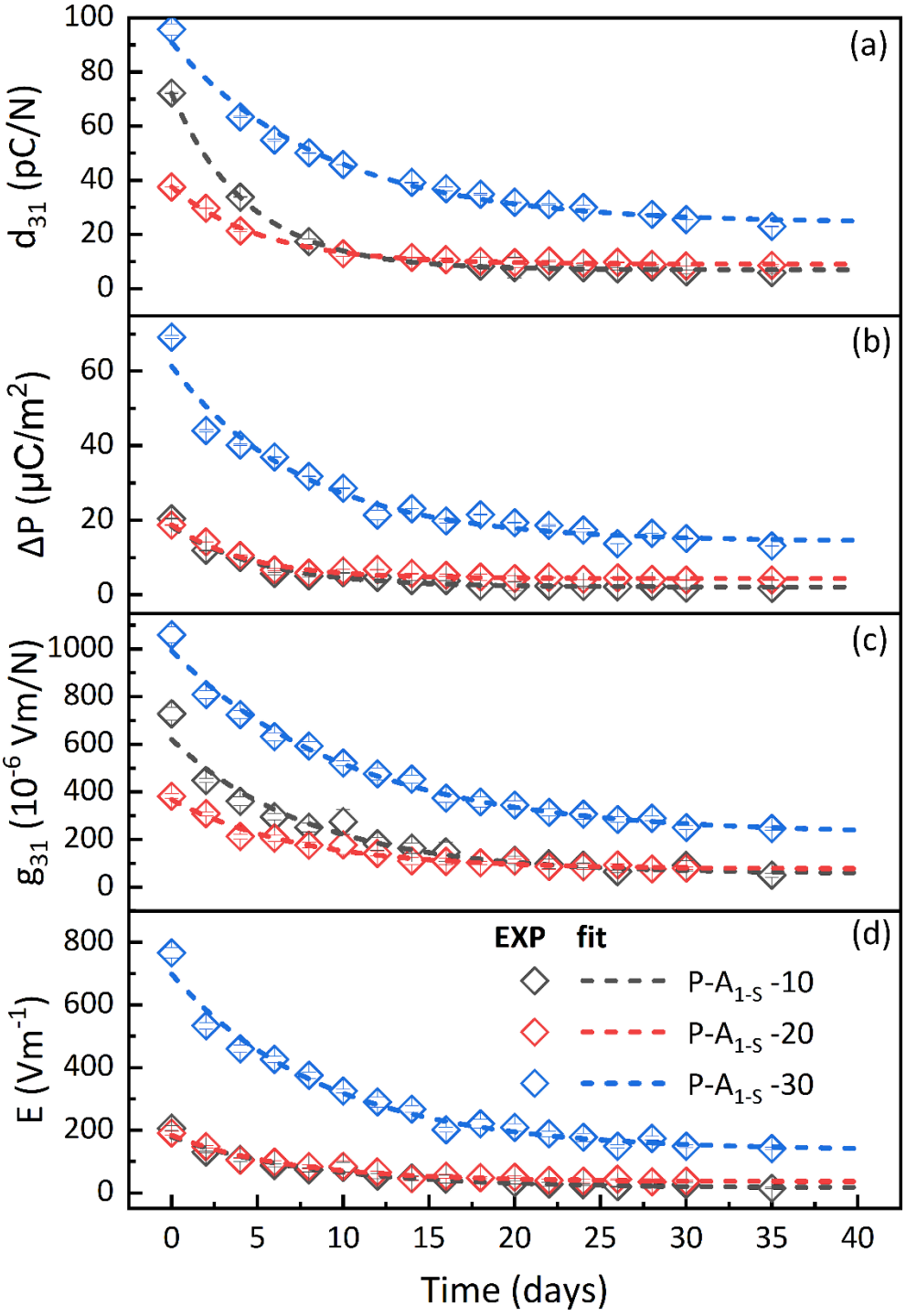

Figure S23 Exponential decay of charges collected at 50% strain deformation cycles over time for composites with increasing filler content and small particle size: (a) calculated transverse piezoelectric charge coefficient, d_{31}; (b) stress-induced polarization, ΔP; (c) estimated transverse piezoelectric voltage coefficient, g_{31} and (d) stress-induced electric field, E

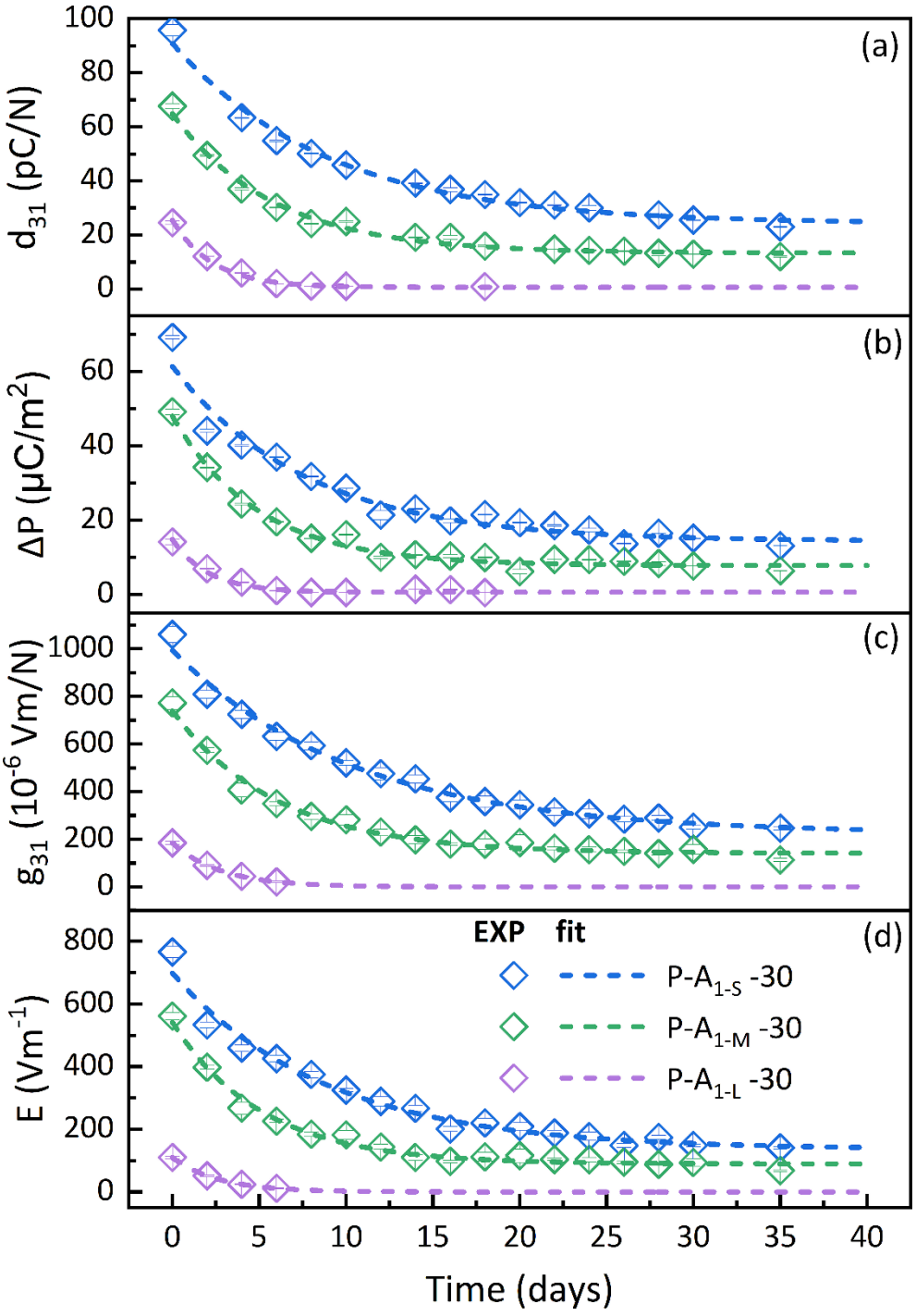

Figure S24 Exponential decay of charges collected at 50% strain deformation cycles over time for 30 wt% composites containing P-$A_1$with changing filler particle size: (a) calculated transverse piezoelectric charge coefficient, d_{31}; (b) stress-induced polarization, ΔP; (c) estimated transverse piezoelectric voltage coefficient, g_{31} and (d) stress-induced electric field, E

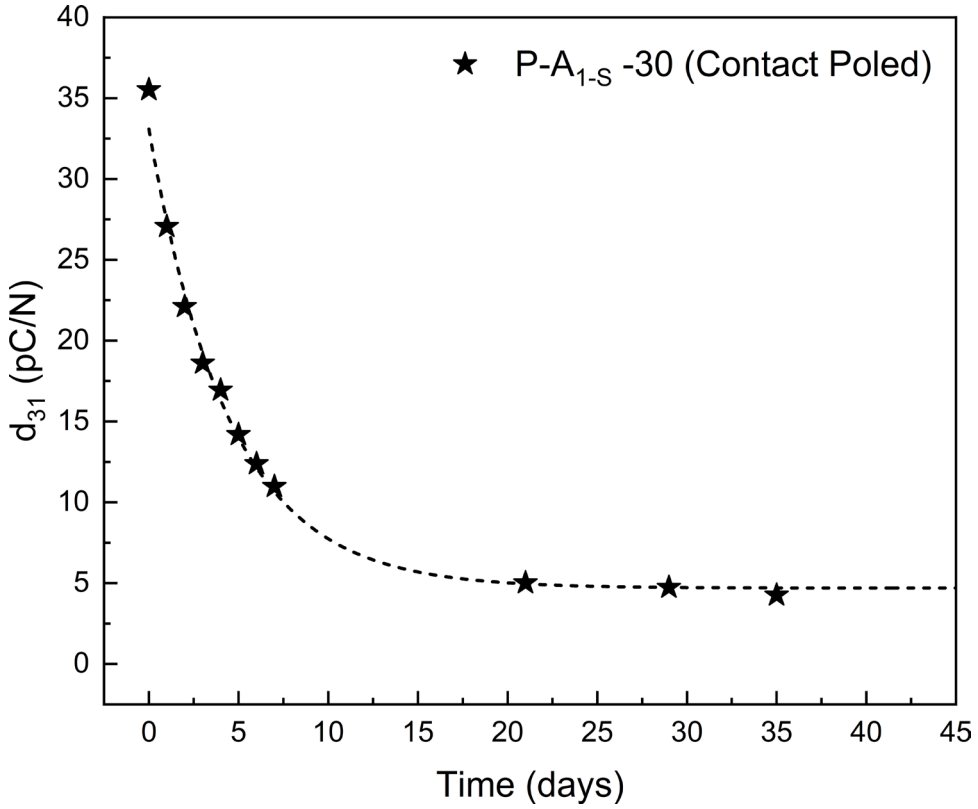

Figure S25 Electrode contact poled specimen of P-$A_{1\text{-}S}$-30; Exponential decay of calculated transverse piezoelectric charge coefficient, d_{31} at 50% strain deformation cycles over time.

References

1. F. Owusu, M. Tress, F. A. Nüesch, S. Lehner, D. M. Opris, *Materials Advances* **2022**, 3, 998

2. Y. S. Ko, F. A. Nüesch, D. M. Opris, *Journal of Materials Chemistry C* **2017**, 5, 1826

3. Z. Ounaies, J. A. Young, J. S. Harrison, in *Field Responsive Polymers*, Vol. 726, American Chemical Society **1999**, Ch. 6, p. 8

4. M. G. Broadhurst, G. T. Davis, *Ferroelectrics* **1984**, 60, 3

5. E. Fukada, *Annals of the New York Academy of Sciences* **1974**, 238, 7.